Integrated Analysis of Scramjet Flowpath with Innovative Inlets

Datta V. Gaitonde and F. Malo-Molina
US Air Force Research Laboratory, Air Vehicles Directorate (AFRL/VA), Computational Sciences Branch, Wright-Patterson AFB, OH
{Datta.Gaitonde, Faure.MaloMolina}@wpafb.af.mil

Houshang B. Ebrahimi
Aerospace Testing Alliance, Inc., Arnold AFB, TN
Houshang.ebrahimi@arnold.af.mil

D. Risha
US Air Force Research Laboratory, Propulsion Directorate (AFRL/PR), Wright-Patterson AFB, OH
Daniel.Risha@wpafb.af.mil

Abstract

Significant progress has been achieved during the first year of this Challenge effort, in developing and simulating configurations which highlight the main scramjet inlet flow path alternatives. In particular, three different types of inward-turning inlets have been explored, including the rectangular cross-section, scoop and "jaws" designs. Each flowpath has been discretized and subjected to inviscid, laminar and turbulent analyses with highly-scalable solvers at design and off-design conditions ranging from Mach 6 to Mach 10. Viscous/inviscid interactions are observed to have a profound impact on the flow, giving rise to distortion of the velocity profile at the exit of the inlet (entrance of the isolator/combustor component). For the jaws approach, the effects of angle-of-attack and yaw have been studied. A complex pattern of low and high total pressure variation is observed, suggesting strategies for the subsequent fuel injection processes. For the rectangular cross-section dual-plane compression inlet, combustor integration has been accomplished with finite-rate chemical kinetics. The effect on mixing characteristics of numerous injection strategies, both upstream and/or in the interior of a wall cavity, are examined. The injection process is observed to yield a separation shock, bow shock and Mach disk, as well as a reattachment shock. Potential phenomena that might generate instabilities and subsequent unstart have been identified, as are locations of high temperature, unburnt fuel gases and combustion efficiency. In a separate, but related effort, simulations have also been performed to yield data for flight-test experiments (HiFIRE program) to ensure survivability of mass capture diagnostic devices.

1. Introduction

The promise of hypersonic air-breathing flight, defined for this purpose as speeds higher than five times that of sound, is well known for both military and commercial applications. From the military standpoint, high-speed vehicles enable new options through rapid-response and kinetic-kill capability, while economic implications become readily apparent when such flight is viewed as a key component of an on-demand access-to-space strategy for satellite launch and servicing. However, the realization of high-speed air-breathing vehicles has been inhibited by many daunting challenges encountered in diverse areas spanning thermal management, hypersonic aerodynamics, aerothermodynamics and aero-propulsion integration. This Challenge effort addresses the last of these difficulties, which arises from the fact that optimized flowpaths do not exhibit the typical delineation between airframe and engine that is possible at low-speeds.

Traditional inlet and propulsion integration tools often oversimplify the non-linear and non-equilibrium phenomena encountered in hypersonic flight, and thus can produce inoperable or inefficient designs. The impact of complex non-ideal fluid dynamic and combustion phenomena on performance is significant, especially when the small operating margins of supersonic propulsion devices is taken into account. Furthermore, separate research performed under a recently concluded challenge effort (C1C) has clarified the effect of distortion in degrading thermal and energy management techniques.

In this Challenge effort, several alternative flow-paths are examined with advanced scalable simulation

0-7695-3088-5/07 $25.00 © 2007 IEEE

approaches. Figure 1 exhibits the particular configurations examined: in the present phase only on the inlet and combustor components are considered. Each variant is the subject of intense current scrutiny for potential application to future vehicle systems. The conceptual vehicle in which each may be integrated is also depicted. The top figure shows the traditional rectangular cross-section flow-path, consisting of sequential pitch and yaw-plane compression and a constant area isolator/combustor with a supersonic cavity combustor. The other approach, utilizing elliptic or circular/annular cross-sections, are shown in the middle and lower parts of Figure 1. The so-called scoop variant of the inward turning inlet consists of a streamlined mass-capture entrance, to which has been added a circular cross-section combustor with cavity flame holder. The "jaws" design is also considered, with the advantage of muted shock/shock interactions, lower wetted area and higher potential efficiency. In the present paper, we focus mainly on the rectangular and jaws designs but preliminary scoop results are also included.

High-fidelity scramjet simulations demand integration of several disciplines, including fluid dynamics, combustion, chemical kinetics and molecular physics. To tackle this extremely difficult problem, the present effort combines world-class expertise resident in the Air Force Research Laboratory (AFRL), Air Vehicles and Propulsion Directorates and Aerospace Testing Alliance (Arnold Engineering Development Center). Members of the team are supported through various Air Force Office of Scientific Research (AFOSR) grants and have previously developed advanced simulation tools to perform pioneering research on many critical science issues anticipated in future hypersonic Air Force concepts. These tools, described further below, include high-fidelity capability to simulate all elements in the above flow-paths, including the broad spectrum of scales encountered in viscous/inviscid phenomena such as shock/boundary layer interactions, Mach disks and vortices, and their impact on fuel injection, multi-phase mixing, combustion.

2. Theoretical and Numerical Formulation

Two different codes, both developed with support from the Department of Defense (DoD) High Performance Computing Modernization Program (HPCMP), have been deployed for the inlet and combustor segments respectively, to exploit the efficiency of each. The Air Vehicles Unstructured Solver is based on the Cobalt framework and is highly scalable. Inviscid fluxes are evaluated with a Godunov scheme, while viscous terms are centered. A point-implicit algorithm is employed for stability. A $k-\epsilon$ model is employed for turbulence closure.

For the combustor, the General Propulsion Analysis Chemical Two-Phase (GPACT) code was employed. Mean steady calculations are obtained with finite-rate chemical kinetics JP8-oxygen and nitrogen-based combustion products using 13 species, including C_2H_2, $C_{12}H_{23}$, CO_2, CO, OH, O_2 O, $H2$, H, H_2O, NO, N and N_2 and 20 reactions. Further details may be found in Reference 1. A range of turbulence closures is employed, with most calculations using the $k-\omega$ model. Large Eddy Simulations are also reported for some cases. In this case, closure of species transport and reaction-diffusion processes occurring at small-scales is carried out using the sub-grid combustion model based on the linear-eddy model (LEM), which has proven appropriate for proper capture of the structure and propagation characteristics of turbulent premixed flames over a wide range of operational parameters. Several multi-phase simulations have also been performed. Lagrangian equations of motion and transport are employed for the life histories of a statistically significant sample of individual droplets. For simplicity, the liquid fuel is assumed to enter the combustor as a fully atomized spray comprised of spherical droplets and effects due to breakup and coalescence are neglected.

3. Inlet Dynamics

Figure 2 depicts the principal shock structure of the rectangular and jaws designs. In each case, in the absence of shock/boundary layer interactions, these shocks are essentially planar. The incoming flow undergoes a sequence of compressions starting from the leading edge of the configuration.

For the rectangular design, the initial compression process is external. Near the wall, the effect of shock/boundary layer interactions is more evident. Figure 3 (left) depicts the situation in a representative shock reflection. The deviation of the impingement location from the design condition, at the corner, is due partly to the displacement effect of the boundary layer, which has a modest impact on shock angles, as well as the spreading associated with the upstream influence of the shock as it enters the boundary layer. These non-ideal effects however are amplified with distance downstream. When separation occurs in this context, there is a potential for the weak-interaction limit to be reached, for choking to occur downstream and possible degradation of isolator performance through distortion as elucidated below. The solution suggests avenues for redesign by configuration alteration or through active and passive control. One ongoing activity in the latter area is the use of porous wall effects.

The evolution of the jaws flowfield has also been examined extensively at off-design pitch and yaw conditions. An example flow profile is shown in Figure 4 (left), which shows pressure contours on a sequence of cross-flow planes. The development of complex separated regions and associated distortion is clearly evident. Figure 4 (right) exhibits the Mach number at a section near the entrance to the combustor for the zero angle-of-attack case. In a manner similar to the rectangular cross-section configuration (Figure 3 [right]), two regions of low energy evolve on the top and bottom regions. This common pattern clearly impacts subsequent fuel injection, mixing and combustor performance.

The genesis of the pattern is more clearly explained in the canonical swept interaction problem comprised of two sharp-fins mounted at angle-of-attack on a plate. Numerous prior simulations have shown that the main features of the flow are those shown in Figure 5 (left). The shock-induced adverse pressure rise separates the incoming boundary layer (blue ribbon) from the surface. Swept interactions, being fundamentally three-dimensional, do not yield a closed bubble. The separated boundary layer does not reattach, but rather warps and the limiting ribbon becomes arch-like. The ejection of low-speed fluid near the surface yields a low total pressure region bounded by entrained fluid from the sides, as shown in Figure 5 (right), where simulations at Mach 8 are compared with experiments performed at NASA Ames.

The cross-flow profiles in the jaws inlet under 3° angle-of-attack and yaw conditions are shown in Figure 6. Broadly speaking, the alteration of the shock structure affects the distortion pattern, both qualitatively and quantitatively. The effect of pitch (Figure 6 [left]) is to modify the relative sizes of the two main separation regions. The top lobe is elongated and exhibits a lower Mach deficit while the lower lobe is compressed in the vertical direction and displays a higher Mach deficit. Small low Mach regions are also evident on the sides of the configuration. The effect of yaw, shown in Figure 6 (right), is more significant. The two lobes are effectively displaced towards the lee side of the configuration while, barring the very near wall region, higher Mach numbers are observed on the right side of the configuration. Further details may be found in References 2 and 3.

Preliminary results with the scoop configuration, under turbulent flow assumptions are depicted in Figure 7. The profile exhibits a curved shock, whose profile varies as the cross-flow plane is moved downstream, demarkating the cross-sectional flow into an upper region at lower post-shock Mach number from the higher speed fluid beneath. Although the laminar scoop flow (not shown) exhibits vortical structures similar to those observed earlier for the jaws and rectangular domains, the turbulent flow does not. This indicates a lack of separation and a relatively higher turbulence level. Current efforts are focused on exploring the uncertainty associated with the turbulence model.

4. Combustor Results

Several simulations have been completed on the rectangular cross-section configuration with JP8 fuel kinetics. A cavity flameholding feature is employed with different injection strategies. In order to highlight the broad features of the simulation, Figure 8 displays Mach number contours and location of liquid fuel droplets emanating normal to a set of spanwise distributed injectors located on the upper wall upstream of the cavity. The droplets of liquid fuel are represented by their size and temperature at which they are burned. The initial diameter of the droplets was assumed to be based on a Sauter Mean Diameter distribution. Interactions of the flow, mixing and penetration of the injection is clearly evident. The initial stages of the droplet lifetime are characterized by a high evaporation rate. Further analysis (not shown) permits evaluation of the dynamics of the reactants (fuel and oxygen) and the two main products (water and carbon dioxide). The cavity recirculation zone transports some of the hot combustion products back toward the combustor face (along the cavity back wall) and ignites the incoming fuel and air as it is mixed in the combustion chamber. The mean temperature in the cavity is close to the stagnation temperature of incoming air flow. These recirculation zones form an exceptionally stable combustion region, with vortex diameter about the size of cavity depth, and are aerodynamically stable over a wide range of fuel-air ratios and inlet temperatures and pressures. Furthermore, the products from the fuel-rich-zone remain within the cavity and drive a stable combustion system.

A more sophisticated arrangement, including fuel injectors on both upper and lower surfaces is shown in Figure 9. The calculated ribbons show the fuel emanating from the injectors, penetrating, mixing and recirculating inside the combustor cavity with the air flow, and subsequently regaining kinetic energy and velocity in the downstream direction. Figure 9 (top) shows static temperature on the upper and lower walls of the combustor and exit nozzle. The hottest regions in the combustor are located at the upper wall of the cavity, zones of recirculation in the wake of the injectors and the flow expansion in the nozzle. Figure 9 (bottom) also displays the location and distinctive layer around the flame perimeter, represented by the mass fraction gradient of the produced CO_2. The inset cartoon highlights the anticipated structure of the plume and associated vortices that are visualized in the simulation. The higher

efficiency observed is associated with the better mixing of fuel with inflow air through turbulence effects.

These results reiterate the need to examine the design space by parametric variation of injector location and injection orientation relative to the freestream direction. To this end, ten simulations were performed with parametric variation of the injection processes and cavity lengths. Three representative cases, denoted 2, 3 and 4 are shown in Figure 10. The schematics in the top row indicate the injector locations which include upstream of the cavity as well as on its forward and reclined backward faces. Case 2 comprises two pairs of injectors within the cavity, with injection momentum in the streamwise/counterflow direction, while in Case 3, the injectors on the ramp are replaced with those at the combustor inlet. In Case 4, additional injectors are placed on the inlet surface, while those in the cavity are removed. Details on other configurations explored may be found in Reference 4. In order to analyze the mixing efficiency without the complication of chemical effects, the study explored both combusting and non-combusting flow patterns. Mass fractions of ethylene fuel for the non-reacting case are shown at selected axial locations in Figure 10. These results illustrate the complex aerodynamic flow interactions that occur within the cavity region as the fuel jet interacts with the freestream air flow within the cavity. As expected, the radial distributions of the ethylene fuel mass fractions vary considerably as a result of the injector locations and injection angles. However, the fuel penetration distances appear to be similar for all cases, indicating that fuel stream penetration is not significantly affected by the injector location. In terms of mixing efficiency, and focusing only on the three cases chosen for exposition here, Case 4 depicts the highest value, greater than 50%. However, additional mixing efficiency may be obtained by enhancing transverse z-direction interaction by mounting injectors on the backward facing step. Case 2 on the other hand is shorter, but more importantly, the injection orientation is counter-productive since it does not contribute to the natural driving motion of the vortex inside the cavity (clockwise).

Other conclusions derived from these calculations may be summarized as follows. In general, upstream oriented injector flow is effective at upstream locations in terms of vertical penetration, but displays relatively poor lateral fuel dispersion. On the other hand, upstream oriented injection at downstream locations shows a tendency for the fuel to move toward the cavity floor, thus inhibiting the mixing of the downstream fuel streams. As anticipated, configurations that yield a relatively closed cavity perform poorly. When reactions are included, stronger shock structures and higher temperatures are observed. Further, separation is more pronounced and a trailing-edge shock wave is also formed where the shear layer reattaches at the angled back wall, thus potentially enhancing chemical reactions. The results also indicate potential unsteady flow-field fluctuations near the fuel injection locations and downstream of the combustor. Similarly, an unsteady combustion environment is observed for normal injection and the interaction of the fuel stream with the cavity vortex. It is evident from these results that optimized injection schemes for cavity flame holding can be evaluated using computation fluid dynamics methodologies.

For flight test support, a broad analysis strategy has been deployed, including axisymmetric and full three-dimensional simulations. In addition to obtaining data on natural transition to turbulence and strong shock/turbulent boundary layer interactions associated with a cylinder/flare juncture, the experiment also includes integrated channel to mimic internal flow for survivability and performance of instrumentation to measure mass capture metrics will be evaluated. The present work has addressed uncertainty and risk reduction by employing different codes, freestream conditions (Mach and Reynolds numbers, angles-of-attack and side-slip), wall thermal conditions, model fidelity (invicid, laminar and multiple turbulence models), potential real gas effects, and stability analyses. Preliminary comparisons with concurrent complementary ground-test data have been made, while post-flight analyses will aid in identification of crucial differences between the flight and ground test environments. Further details may be found in Reference 5.

5. Significance to DoD

High-speed vehicles capable of survivable atmospheric (air-breathing) flight enable transformational capability by facilitating conventional munitions strike with adaptive target selection, establishment of adversary exclusion zones and global strike ability with CONUS based assets. Air Force capability focused efforts targeting these future environment drivers, call for creation of desired effects anywhere on the globe within hours of tasking with the ability to plan en route to the mission.

This Challenge effort is examining multiple delivery modes for different missions, including sustained hypersonic cruise and expendable standoff. For these DoD objectives, cost considerations and the difficulty of ground and flight testing, demand the early incorporation of simulation and modeling in the development procedure. The present effort fulfills this requirement, by providing timely high-fidelity analyses of fundamental phenomena, by identifying key limitations on hypersonic air-breathing propulsion through vetting of inefficient or unworkable concepts and by providing lessons-learned

experience at minimal costs. The tools employed have been exhaustively validated by careful comparison with experimental data on canonical configurations, and further, has been made extremely efficient on massively parallel systems, through prior Common High Performace Computing Software Support Initiative and HPC support. By applying this state-of-the-art simulation capability, the DoD will augment its experimental test matrix with simulation-led conceptual and detailed design of the next-generation of high-speed vehicles and access-to-space options. By reducing the wall clock time, the massively parallel simulation strategy fosters the generation and testing of innovative solutions which can preclude costly technological surprises at advanced stages of the program.

Systems Used

NAVO SP4+, ASC SGI O3K, AHPCRC X1

Personnel

D.V. Gaitonde, H. Ebrahimi, E. Josyula, F. Malo-Molina, P. Morgan, J. Poggie, D. Risha, D. Rizzetta, and M. Visbal.

Computational Technology Areas

Computational Fluid Dynamics (70%), and Computational Electromagnetic Acoustics (30%).

References

1. Ebrahimi, H., R. Mohanraj, and C. Merkle, "Multi-Level Analysis of Pulsed Detonation Engines." *Journal of Propulsion and Power*, Vol. 18, pp. 225–232, April 2002.

2. Malo-Molina, F., D. Gaitonde, H. Ebrahimi, and S. Ruffin, "Analysis of an Innovative Inward Turning Inlet Using an Air-JP8 Combustion Mixture at Mach 7." *AIAA paper 2006-3041*, June 2006.

3. Malo-Molina, F., D. Gaitonde, H. Ebrahimi, and S. Ruffin, "Analysis of a Hypersonic Inward Turning Inlet followed by a TVC Using an Air-Hydrocarbon Fuel Mixture." *AIAA Paper 2006-4683*, July 2006.

4. Ebrahimi, H., D. Gaitonde, and F. Malo-Molina, "Parametric Study of 3-D Hydrocarbon Scramjet Engine with Cavity." *AIAA Paper 2007-0645*, Jan 2007.

5. Gaitonde, D., R. Kimmel, D. Jackson, and X. Zhong, "CFD Analysis in Development of Flight Test Article for Basic Research." *AIAA Paper 2006-8085*, 2006.

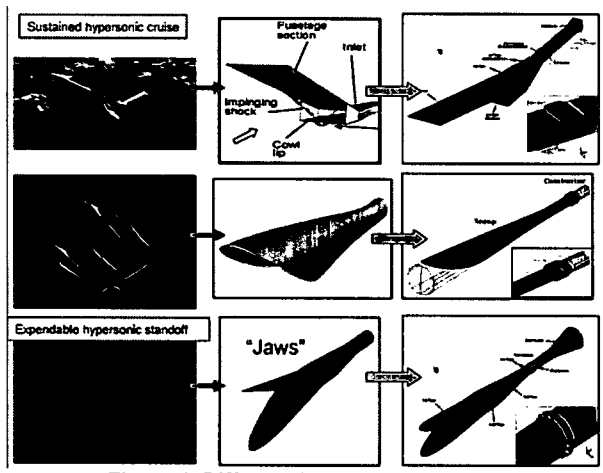

Figure 1. Different flowpaths examined

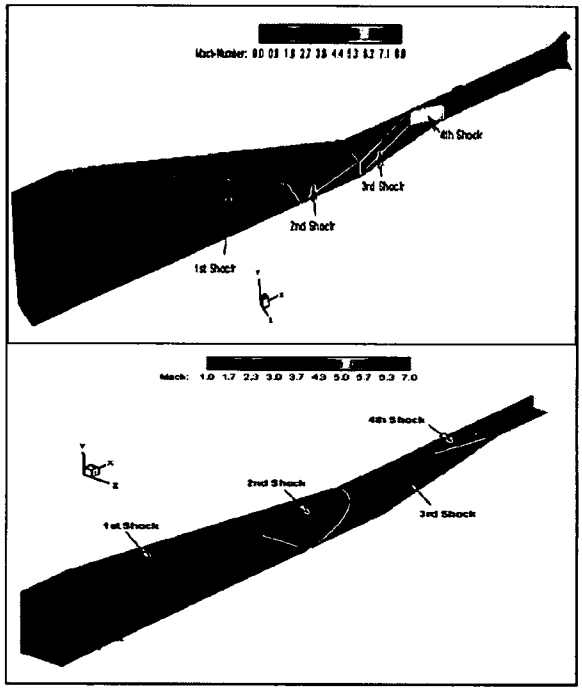

Figure 2. Shock structure in rectangular (top) and jaws configurations (bottom)

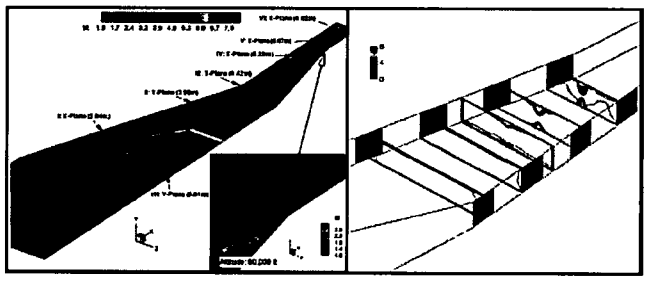

Figure 3. Effect of viscous/inviscid interactions on rectangular inlet. Left: Shock boundary layer interaction at corner, Right: Evolution of vortical structures with distance.

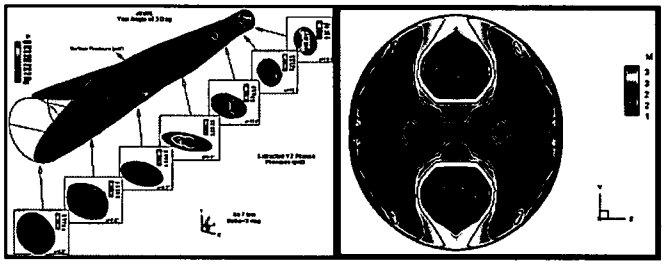

Figure 4. Effect of viscous/inviscid interactions in Jaws configuration. Left: Evolution of distorted flow, Right: Mach number at combustor entrance

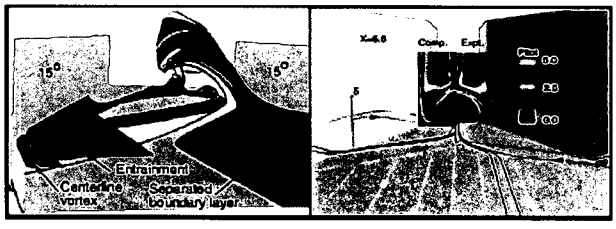

Figure 5. Genesis of low-energy vortical structure due to boundary layer separation. Left: Ribbons of main regimes, Right: Pitot pressure on cross-flow plane.

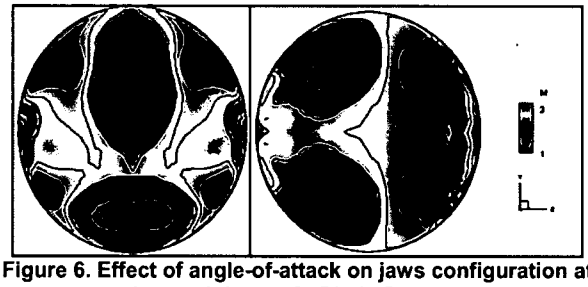

Figure 6. Effect of angle-of-attack on jaws configuration at combustor inlet. Left: Pitch, Right: Yaw.

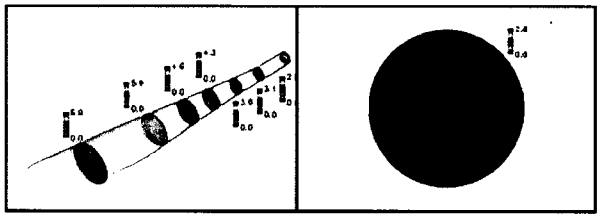

Figure 7. Turbulent flow features in scoop configuration

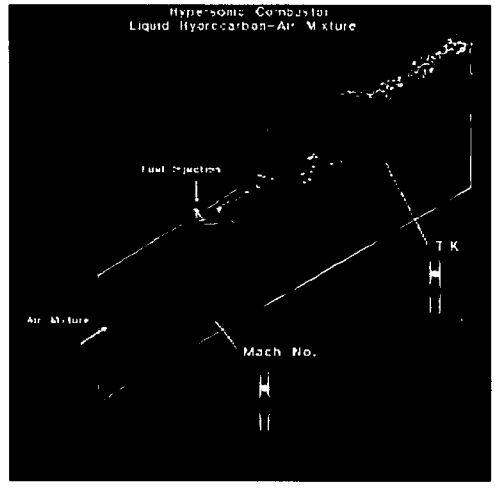

Figure 8. Mach number contours at the center of the injector and the temperature of liquid fuel (JP8) droplets showing breakup and burning downstream in the combustor

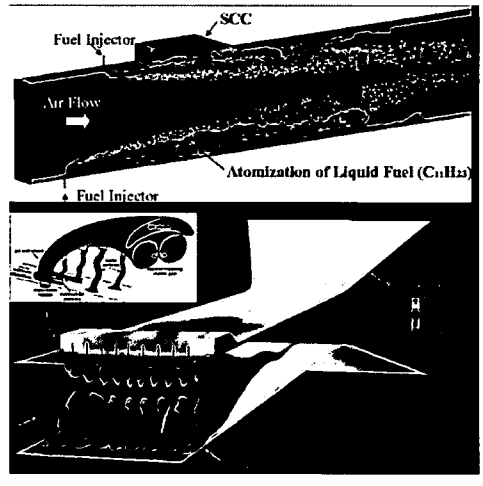

Figure 9. Top: Mach Number contours at the center of the injector and the temperature of liquid fuel (JP8) droplets showing breakup and burning downstream in the combustor, Bottom: Illustration of the flame location using the CO_2 gradients and temperature contour at the walls

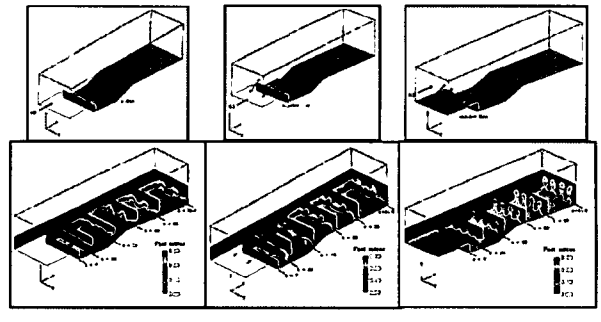

Figure 10. Top: Injection location and orientation schematic. Bottom: Fuel mass fraction contours at the mid X-Z plane and at several cross-sectional Y-Z planes within the combustor.